JOURNAL OF MATERIALS SCIENCE 17 (1982) 1247–1268

A comparison of failure predictions by strength and fracture mechanics techniques

B. J. PLETKA*, S. M. WIEDERHORN
National Bureau of Standards, Washington, D. C., 20234, USA

Predictions of lifetime under load were made for five ceramic materials using strength and fracture mechanics techniques. The double-torsion technique was used to obtain fracture mechanics data, while the stressing-rate technique was used to obtain strength data. An error analysis based on the error propagation law was performed to determine confidence limits for the failure predictions. Agreement of lifetime predictions by the stressing-rate and fracture mechanics techniques were obtained for only two of the materials. The implications of these results with regard to microstructural effects on crack propagation and design applications are discussed.

1. Introduction

The ultilization of ceramic materials in structural applications is often hampered by the inherent brittle nature of these materials, which results in a substantial variability in strength, and a time dependence in strength known as static fatigue. Although it has been recognized for many years that these effects of brittle behaviour are due to small cracks or other flaws normally present in ceramic materials, design techniques have been developed only recently to improve the structural reliability of these materials.

Design methods for ceramic materials are based on the premise that failure results from the growth of cracks that are present either in the surface or volume of the material. When one of the growing cracks reaches a critical size, failure is almost instantaneous. The strength of the ceramic is determined primarily by the initial size and shape of the crack that causes failure. Consequently, the scatter that is observed in the strength of ceramics is due to the scatter in the size and shape of the initial cracks present in the ceramic, and the time required for a component to fail when subjected to a load is the time necessary for a crack to grow from the initial size to the final critical size.

Techniques of predicting the strength of ceramic materials are based on the theory of fracture mechanics [1–4]. This theory provides a means of characterizing the stress field in the vicinity of a crack tip and thus the driving force for crack growth. Using the theories of fracture mechanics, the conditions for both crack growth and critical crack size can be established. The theory also relates these conditions to experimental parameters that can be obtained by standard experimental techniques for measuring strength or crack growth rates. With regard to failure prediction, the main consequence of fracture mechanics theory is that the lifetime under load can be predicted from two sets of experimental parameters: one that characterizes the crack growth; the other that characterizes the initial size of the cracks that cause failure.

Measurements that are used to characterize crack growth rates are conducted on laboratory specimens that have the same chemical composition and microstructure as the components. A basic assumption of the theory used for design is that for a given environment the crack growth parameters determined from such measurements depend only on composition and microstructure, but not on the type of measurement used to determine the crack growth parameters. The main objective of this paper is to present the results of a study to test this assumption. It is

*Present address: Department of Metallurgical Engineering, Michigan Technological University, Houghten,Michigan 49931, USA.

0022–2461/82/051247–22$05.14/0

shown that the assumption is a weak link in the theory, and that crack growth parameters determined by different techniques can differ substantially. Consequences of this finding are discussed with regard to lifetime predictions for ceramic materials.

2. Theoretical background

Parameters used to characterize subcritical crack growth in ceramic materials can be evaluated either by direct crack-velocity measurement techniques, or by strength measurement techniques [5, 6]. Regardless of which technique is used, it is commonly found that the crack velocity, v, can be expressed as a power function of the applied stress intensity factor, K_I:

$$v = v_0 (K_I/K_0)^n, \quad (1)$$

where v_0 and n are environmentally dependent materials constants, and K_0 is an arbitrary constant used to normalize K_I*. K_I is defined in terms of the applied stress σ and the crack length, a: $K_I = \sigma Y\sqrt{a}$, where Y is a constant determined by the geometry of the crack.

By assuming that failure is due to subcritical crack growth from a pre-existing flaw, the time to failure, t, can be calculated for a component subjected to a constant applied stress, σ_a [2, 4]:

$$t = BS_i^{n-2}\sigma_a^{-n}, \quad (2)$$

where S_i is the initial strength and B is a constant, S_i is defined in terms of the size, a_i, of the critical flaw that causes failure:

$$S_i = K_{IC}/(Y\sqrt{a_i}), \quad (3)$$

where K_{IC} is the critical stress intensity factor, a materials constant that defines the value of K_I at which the crack velocity increases precipitously as the crack grows larger. The value of the constant Y ranges from $\sqrt{\pi}$ for a two-dimensional through-crack to $(4/\pi)^{1/2}$ for a penny-shaped crack. The strength, S_i, can be measured experimentally by loading the component to failure in such a way that subcritical crack growth does not occur during the fracture test. Measurement of S_i is usually done in an inert environment using rapid loading rates to minimize subcritical crack growth before failure.

The constant, B, in Equation 2 can be evaluated experimentally, either by using fracture mechanics techniques, or by using strength measurement techniques. As shown by the following equation, the constant B can be expressed solely in terms of constants determined by fracture mechanics experiments [4, 7]:

$$B = (2K_0^n)/[v_0 Y^2 (n-2)K_{IC}^{n-2}], \quad (4)$$

where each of the above terms has already been defined. Thus the constant B depends on n and v_0, which are determined from crack growth studies, and on K_{IC}, which is evaluated from fracture toughness measurements.

The constants B and n can also be determined from experiments in which the time to failure of a set of laboratory specimens is measured as a function of applied stress, σ_a. Expressing Equation 2 in logarithmic form,

$$\ln t = \ln (B S_i^{n-2}) - n \ln \sigma_a, \quad (5)$$

where n is evaluated from the slope of a plot of log t against ln σ_a, while B is evaluated from the intercept of such a plot. The strength, S_i, is determined from a separate set of strength measurements. To fit Equation 5 to a set of experimental data, median or mean values of S_i, t and σ_a are usually used.

The constants B and n can also be determined from constant stressing-rate experiments. In this type of experiment, the breaking stress, σ_f, of a set of components is determined as a function of the stressing rate, $\dot{\sigma}$. An analysis of this type of experiment yields the following relationship between these two variables [4, 6, 7]:

$$\ln \sigma_f = (n+1)^{-1} \ln [B(n+1) S_i^{n-2}] + (n+1)^{-1} \ln \dot{\sigma}. \quad (6)$$

The constant n is evaluated from the slope of a logarithmic plot of σ_f against $\dot{\sigma}$, while B is evaluated from the intercept of such a plot. Again, S_i is determined in a separate set of experiments, and median or mean values of σ_f and S_i are used to fit Equation 6 to the experimental data.

Once n and B have been evaluated, they can be substituted into Equation 2 to estimate the failure time. For practical applications, n and B are evaluated on laboratory test specimens. The values of n and B should not depend on the experimental technique used for their evaluation, provided they are, in fact, material–environment constants. Furthermore, the failure time calculated from

*In the present study, the value assigned to K_0 was 1 Pa m$^{1/2}$.

Equation 2 should not depend on the technique used to evaluate n and B. At present, some experimental data support the assumption that the propagation of large flaws in fracture mechanics specimens and small flaws in strength specimens are equivalent [8–14], while other experimental data do not support this assumption [12, 13, 15]. In this paper, an evaluation of these failure prediction theories for five ceramic materials was undertaken using both fracture mechanics and strength measurement techniques. The intent of this study was to test the limits of the theory and to suggest guidelines for the implementation of the theory for purposes of lifetime prediction.

A useful graphical method of comparing failure-time predictions based on values of n and B determined by different experimental techniques can be obtained by a slight modification of Equation 2. Rearranging the equation and expressing it in logarithmic form, *

$$\ln (t\,\sigma_a^2) = \ln B + (n-2) \ln (S/\sigma_a), \quad (7)$$

a modified failure time, $t\sigma_a^2$, is expressed as a function of the ratio of the initial strength to the applied stress, S/σ_a. The intercept of this equation is given by $\ln B$ while the slope is given by $(n-2)$. This type of representation of static fatigue data is useful for comparing data collected on different kinds of materials, or for comparing different techniques used to collect static fatigue data on a single material. In this paper, Equation 7 is used for the latter purpose.

3. Experimental procedure

Crack growth parameters B and n were evaluated for five different ceramic materials using both constant stressing-rate and fracture mechanics techniques. Lifetime predictions based on these measurement techniques were compared using Equation 7. The ceramics studied were: an ultra-low expansion glass (C7971); two glass-ceramic (Pyroceram C9606 and Cervit 126) and two grades of high-density aluminium oxide (Wesgo Al-300, 9 μm and 18 μm grain size).* The Cervit 126 was obtained from Keopke and is the same material used by him in an earlier fracture study [16].

Fracture mechanics data were collected using double torsion specimens that were 2 mm by 25 mm by 75 mm [17–19]. To control the direction of crack growth, a side groove approximately 2 mm wide and 1 mm deep was ground parallel to the longest dimension of the specimen, along the specimen mid-plane. A majority of tests were conducted with the groove on the tensile surface of the specimen. Crack velocity data were obtained using the load relaxation method on specimens that were precracked and tested in distilled water. Usually, several relaxation runs were made on each specimen. Values of n and $\ln v_0$ (Equation 1) were obtained from a linear regression analysis of $\ln K_I$ upon $\ln v$ for each load relaxation measurement; this procedure minimized the error in $\ln K_I$. Because extraneous effects can occur with the double-torsion technique (e.g. load relaxation not due to crack growth; intersection of the crack with the side-wall of the groove), the experimental precautions outlined in [17] were followed scrupulously in this investigation.

Measurements of the fracture toughness, K_{IC}, were also made using double-torsion specimens. To avoid subcritical crack growth as a result of water at the crack tip, all specimens were placed in an oven at 100° C for a period of approximately 20 h prior to testing, and tests were conducted in an enclosed chamber through which dry N_2 was passed for at least 15 min prior to testing. The load was applied at a constant, cross-head speed in the range 0.2 to 0.5 cm min^{-1}. The peak load was used to evaluate K_{IC}.

With the exception of Cervit 126, strength measurements were made using both the four-point bending technique and a biaxial bending technique developed originally by Wachtman *et al.* [20]. The Cervit 126 glass-ceramic was tested using only the biaxial tension technique. Four-point bend specimens for the Pyroceram

*Equation 7 is an approximation which holds as long as $(S/\sigma_a)^{n-2} \gg 1$. In the more complete expression $(n-2) \ln S/\sigma_a \rightarrow \ln [(S/\sigma_a)^{n-2} - 1]$. For most practical applications, Equation 7 (and Equation 2) are adequate for purposes of lifetime predictions. Note that the subscript i has been dropped from the initial strength in Equation 7. S_i is used to identify initial strengths in laboratory experiments which are used to evaluate B and n. S_i is measured in the laboratory by destructive testing. The inert strength of components that are to be used for engineering applications have to be measured by other means. Hence, the two inert strengths have to be identified separately. Predictive equations in this paper use S without subscript i to identify the inert strength of engineering components.

*The use of these commercial designations is for identification purposes only and does not indicate endorsement by the National Bureau of Standards.

and the 18 μm aluminium oxide were made from the same billets as the double-torsion specimens, whereas specimens for the glass and the 9 μm aluminium oxide were made from the double-torsion specimens after they had been tested. Although the strength specimens varied somewhat in dimensions, all were tested in distilled water on a fixture with 50 mm outer span and a 10 mm inner span. As a final step in the machining process, a 400 mesh diamond-grit grinding wheel was used to produce a uniform surface finish on all four-point bend specimens.

Fracture strength measurements were made at five different stressing rates (a decade apart), except for the Pyroceram for which seven stressing rates were used. For all materials studied, at least 10 specimens were broken at each stressing rate. Specimens used to determine the inert strengths were dried in a manner that was identical to that used for the double-torsion specimens, and were fractured at the highest stressing rate used for specimens tested in water.

Biaxial tension strength measurements were made on all materials used in this study. Specimens were discs 1 to 1.5 mm thick and approximately 32 mm in diameter. They were cut from the same billets as the fracture mechanics specimens, and with the exception of the glass, were ground with a 400 mesh diamond wheel. Polished specimens were used for the glass. Discs were supported on three spherical steel bearings, equi-spaced on a 12.7 mm radius, and were centre loaded by a 1.6 mm diameter ram. Test procedures for the discs were identical to those used for the four-point bend specimens. The constant stressing-rate experiments were conducted in distilled water, while inert strength measurements were conducted in a flowing stream of dry nitrogen.

To determine the values of the constants used in Equation 7, a linear regression analysis was applied both to the crack growth data, and to the strength data. For the crack growth data, n and $\ln v_0$ were evaluated for each run by a linear regression of $\ln K_I$ upon $\ln v$. Since several crack velocity curves were obtained for each specimen, the n and $\ln v_0$ used to characterize each curve were treated as statistically independently determined constants. For each material tested, an average value of n and $\ln v_0$ ($\langle n \rangle$, $\langle \ln v_0 \rangle$) was determined from the values obtained from each experimental curve. These average values were assumed to be the best estimate of n and $\ln v_0$. As shown in the Appendix, the average values of n and $\ln v_0$ were used to evaluate the variance and covariance of n and $\ln v_0$. These estimates of the variance and covariance were used to establish 95% confidence limits for Equation 7, thus facilitating intertest comparisons for a given material.

Strength measurement data were treated somewhat differently from crack velocity data. For each stressing rate, $\dot{\sigma}$, the median value of the breaking stress, σ_f, was determined. A linear regression analysis of $\ln \sigma_f$ upon $\ln \dot{\sigma}$ was then used to obtain an estimate of n, $\ln B$, the variance of n and $\ln B$, and the covariance of n and $\ln B$ [cov (n, $\ln B$)]. As with the crack propagation studies, these statistical parameters were used to establish 95% confidence limits for Equation 7.

4. Results

4.1. Fracture mechanics measurements

Data summarizing the crack growth behaviour and fracture toughness of each material are presented in Table I of this paper. The variance of $\langle n \rangle$ and $\langle \ln v_0 \rangle$ are included in Table AI of the Appendix.

The crack growth data for the ultra-low expansion glass were obtained earlier, primarily by the double-cantilever beam technique [8]. Since data on the other materials shown in Table I were obtained by the double-torsion technique, additional measurements were made on the ultra-low-expansion glass to assure ourselves that the data from these two techniques were in fact

TABLE I Fracture mechanics measurements

Material	n	$\ln v_0$	K_{IC} (MPa m$^{1/2}$)
Ultra-low-expansion glass (C7971)	35.0 (1.9)*	−470	0.70 (0.03)
Pyroceram glass-ceramic (C9606)	83.5 (6.8)	−1224	2.32 (0.10)
Cervit 126 glass-ceramic	45.5 (10.2)	−625	0.90 (0.08)
9 μm Al_2O_3	104.1 (18.8)	−1583	4.35 (0.22)
18 μm Al_2O_3	111.3 (21.9)	−1724	6.81 (0.32)

*The numbers in parentheses are the standard deviation. Other statistical parameters are listed in Table AI in the Appendix.

compatiable for this glass. Two load relaxation experiments (by the double-torsion technique) on the ultra-low-expansion glass yielded values of 36.0 and 32.2 for n. Since these values of n agreed with the average value of 35.4 obtained by the double-cantilever technique, they were pooled with the earlier set of data to give the values shown in Table I.

Typical crack velocity data on the glass ceramics (Pyroceram; Cervit 126) show a systematic shift of the crack velocity curves to lower values of K_I as the crack length increases (Fig. 1). This dependence of the v–K_I curves on crack length is supported by a preliminary experimental study of these materials [21], by a three-dimensional finite-element analysis of the double-torsion technique [22] and by other experimental studies [17, 23]. The data collected by the double-torsion technique were taken from specimens that contained crack lengths that were greater than the width of the specimen, > 25 mm, to avoid anomalous effects (high values of n and large systematic shifts in K_I) that have been reported for this technique [17]. Despite these precautions, a small systematic shift in the crack velocity curve to lower values of K_I was observed in our study. This procedure of restricting our study to cracks that were greater than 25 mm did, however, reduce the scatter of the v–K_I data and avoid the inclusion of unusually high values of n in the data pool. Crack propagation studies on the fine-grain (9 μm) aluminium oxide ceramic indicated that the fracture behaviour of this material was very similar to that of the glass-ceramics. Again, systematic shifts in the v–K_I curves to lower values of K_I were observed as the crack length increased (Fig. 2).

In contrast to the other materials used in this study, considerable difficulty was encountered in the collection of crack growth data on the large-grained (18 μm) aluminium oxide. Cracks in this material often propagated into the wall of the side groove where they became trapped. This behaviour resulted in anomalous crack propagation curves which appeared to approach a fatigue limit at high values of K_I. The data clearly did not represent the crack propagation behaviour of the material under

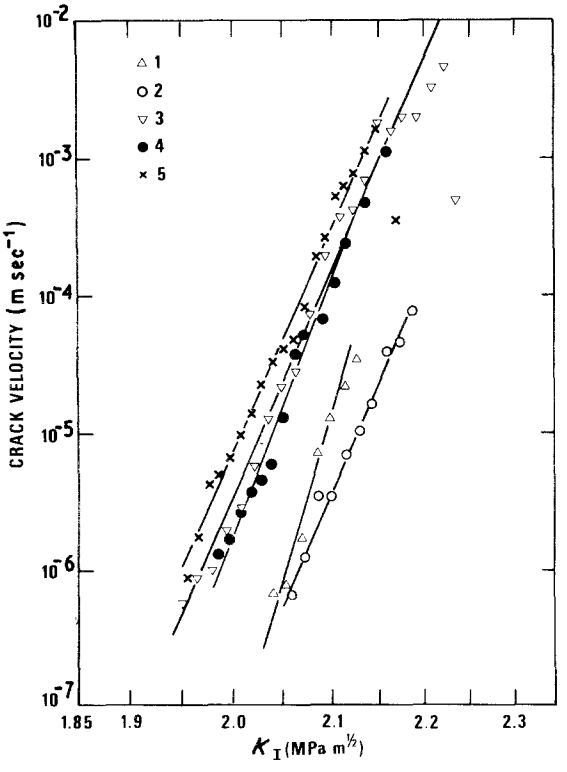

Figure 1 Crack velocity as a function of applied stress intensity factor for five stress relaxation experiments (identified in upper left of figure) on the same Pyroceram glass-ceramic specimen.

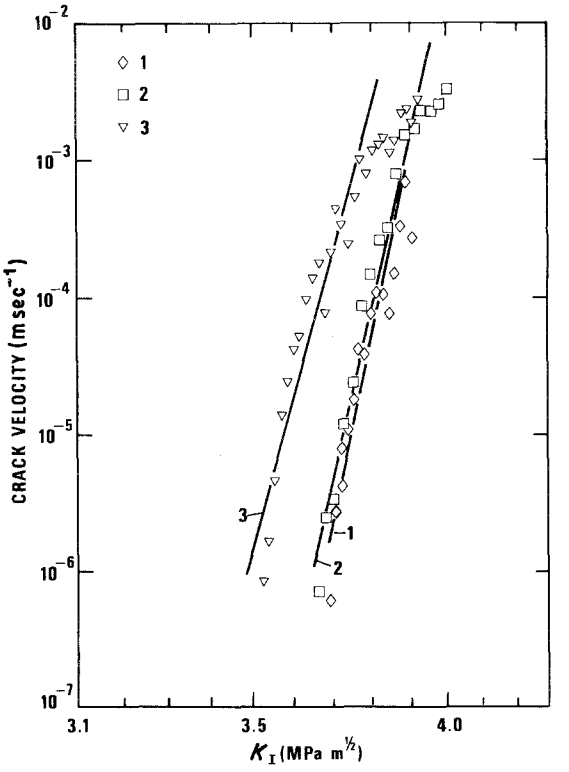

Figure 2 Crack velocity as a function of applied stress intensity factor for three stress relaxation experiments (identified in upper left of figure) on the same 9 μm grain-size alumina specimen.

study. To obtain representative crack growth data on the large-grained aluminium oxide, each specimen was examined by optical microscopy after each run to determine whether the crack had intersected the wall of the side groove during crack growth. Table I contains only those sets of data that were obtained from specimens in which the crack did not intersect the wall of the side groove. In general, crack propagation data that were acceptable exhibited a substantial relaxation of the load during the crack growth study.

The anomolous behaviour of the large-grain aluminium oxide is undoubtedly related to the meandering nature of the crack path in this material. As can be seen in Fig. 3d, cracks followed a much more tortuous path in the large-grained aluminium oxide than in the other materials studied. This behaviour is probably the result of a strong interaction between the crack front and the microstructure of this material. The large grains of aluminium oxide can apparently cause large deviations in the crack propagation direction, which results in frequent intersection of the crack with the walls of the groove. Examination of the crack paths of the other materials used in this study, see Fig. 3a to c, indicates a similar meandering behaviour of the crack path. However, because of the small grain size in these materials, the crack path approximates a straight line and, as a consequence, crack intersection with the walls of the groove was not a problem.*

4.2. Strength measurements

Measurements of the breaking stress as a function of stressing rate were conducted using both four-point bending and biaxial tension strength measure-

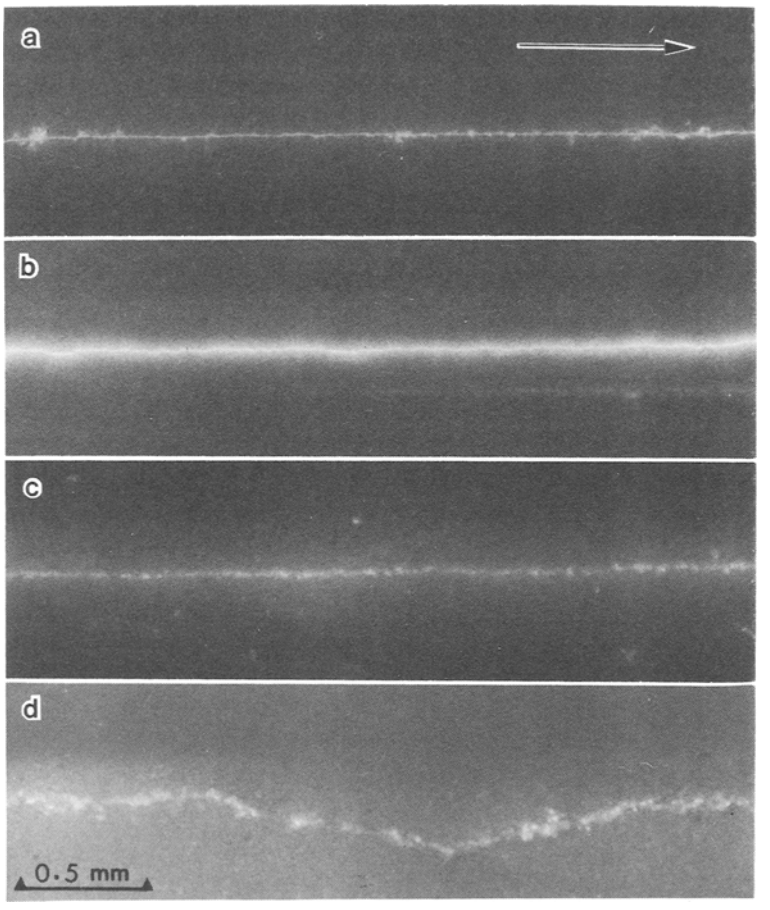

Figure 3 Optical micrographs of crack morphology for the leading crack edge in (a) Cervit 126 glass-ceramic, (b) Pyroceram glass-ceramic, (c) 9 μm grain-size alumina and (d) 18 μm grain-size alumina. Arrow indicates crack propagation direction.

*It is worth noting that crack intersection with the walls of the groove could have occurred in any of the materials studied. Provided the specimen is well-aligned in the test fixture, intersection of the crack with the groove walls is much less likely if the crack is straight. In an earlier study on Pyroceram [21], the crack branching and crack arrest that was reported was in fact the result of intersections with the walls of the side groove. This fact was only recognized after publication of the earlier paper.

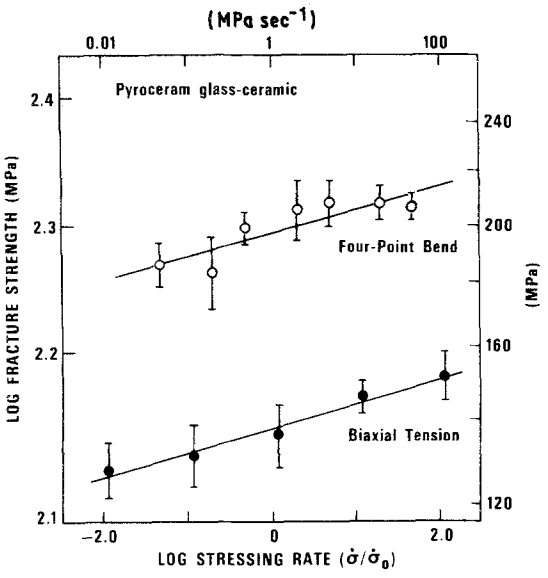

Figure 4 Fracture strength as a function of stressing rate for Pyroceram glass-ceramic in distilled water at room temperature. Bars represent 95% confidence limits.

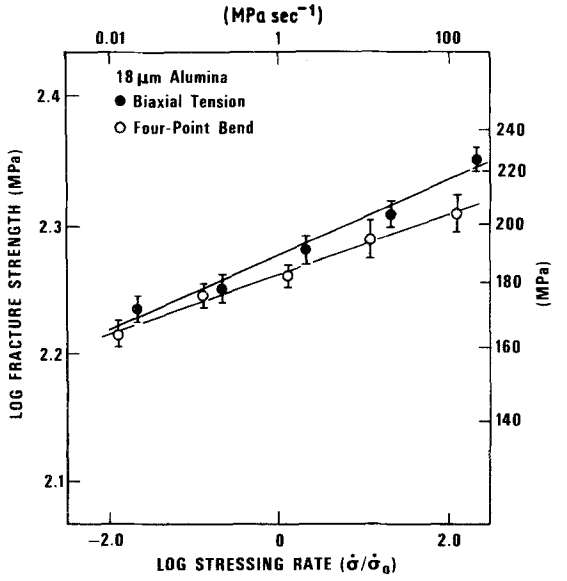

Figure 5 Fracture strength as a function of stressing rate for 18 μm grain-size alumina in distilled water at room temperature. Bars represent 95 % confidence limits.

ment techniques. The types of data obtained in these studies are illustrated in Figs 4 and 5. The error bars for these data represent 95% confidence limits for each stressing rate.

In general, the data can be represented by a straight line on a logarithmic plot of breaking stress as a function of stressing rate. The quality of the fit to the straight line depends on the material tested and the type of strength test employed (i.e. four-point bend or biaxial tension). Of the materials studied, the 18 μm aluminium oxide data seemed to give the best fit to a straight line. For this material, the deviation about the mean breaking stress was approximately 3% for each breaking stress. By contrast, the Pyroceram gave the poorest fit to a straight line. The scatter of the data about the regression line, and the standard deviation of the breaking stress (5 to 10% of the mean) were both larger for the Pyroceram than for the 18 μm aluminium oxide. Data from the other materials fell within the range represented by Figs 4 and 5.

A summary of the data obtained from the stressing-rate experiments is presented in Tables II and III, which give the linear regression coef-

TABLE II Summary of crack propagation data determined from biaxial strength measurements

Material	n	$\ln \sigma_{f_0}$	S_i (MPa)
Ultra-low-expansion glass (C7971)	26.9 (3.6)*	18.238	230.1 (38.3)
Pyroceram glass-ceramic (C9606)	46.3 (6.4)	18.440	195.7 (12.6)
Cervit 126 glass-ceramic	32.9 (2.3)	17.954	126.7 (4.2)
9 μm Al_2O_3	33.8 (1.7)	18.916	380.6 (16.7)
18 μm Al_2O_3	34.5 (4.1)	18.668	296.6 (15.8)

*The numbers in parentheses are the standard error for n and the standard deviation for S_i. Other statistical parameters are listed in Table AII in the Appendix.

TABLE III Summary of crack propagation data determined from four-point bend strength measurements

Material	n	$\ln \sigma_{f_0}$	S_i (MPa)
Ultra-low-expansion glass (C7971)	33.3 (1.8)	17.469	88.5 (14.0)
Pyroceram glass-ceramic (C9606)	62.5 (13.6)	18.893	246.2 (10.3)
9 μm Al_2O_3	49.3 (11.7)	19.130	350.8 (18.5)
18 μm Al_2O_3	39.2 (0.9)	18.678	280.5 (15.8)

*The numbers in parentheses are the standard error for n and the standard deviation for S_i. Other statistical parameters are listed in Table AIII of the Appendix.

TABLE IV Calculated intercept on failure prediction diagrams ($\ln B$)

Material	Crack growth	Biaxial tension	Four-point bend
Ultra-low-expansion glass (C7971)	21.9115	26.086	22.908
Pyroceram glass-ceramic	24.5942	22.576	26.594
Cervit 126 glass-ceramic	24.382	28.606	-
9 μm Al_2O_3	13.782	24.446	27.659
18 μm Al_2O_3	−0.8609	25.138	23.544

ficients for the strength data obtained from the biaxial tension and the four-point bend tests, respectively. The constant n and $\ln \sigma_{f0}$ and the standard error of n are given in Tables II and III for the median fracture stress. A similar set of data was obtained for the mean value and standard deviation of the fracture stress. Applications of a Student t-test of these sets of data suggests that there is little difference between the constants n and $\ln \sigma_{f0}$ obtained by the two types of linear regression analysis (i.e. the mean fracture strength against the median fracture strength). Since it apparently makes little difference as to whether the mean or median values of strength are used for the regression analysis, the linear regression coefficients obtained from the median values of the strength are used for the lifetime prediction equations. Other experimental parameters needed for lifetime predictions and for estimating the variance of those predictions are given in Tables AII and AIII of the Appendix.

4.3. Failure prediction diagrams

As noted in Section 2 of this paper, Equation 7 can be used to test the premise that n and B are materials constants that do not depend on their method of evaluation. As shown in the Appendix (Equation A7) the value of $\ln B$ can be obtained from the regression coefficients of the stressing-rate data and from measurements of the inert strength by using the following equation:

$$\ln B = (n+1)\ln \sigma_{f0} - (n-2)\langle \ln S_i \rangle - \ln(n+1) - \ln \dot{\sigma}_0. \quad (8)$$

The value of $\ln B$ can also be obtained from crack growth data by using Equation 4. Values of B obtained in this manner are given in Table IV and are used in Figs 6 to 10 to plot $\ln(t\sigma_a^2)$ as a function of $\ln(S/\sigma_a)$. As can be seen from Figs 8 to 10, obvious agreement between the techniques used for lifetime prediction is obtained for the low-expansion glass, for the two sets of strength

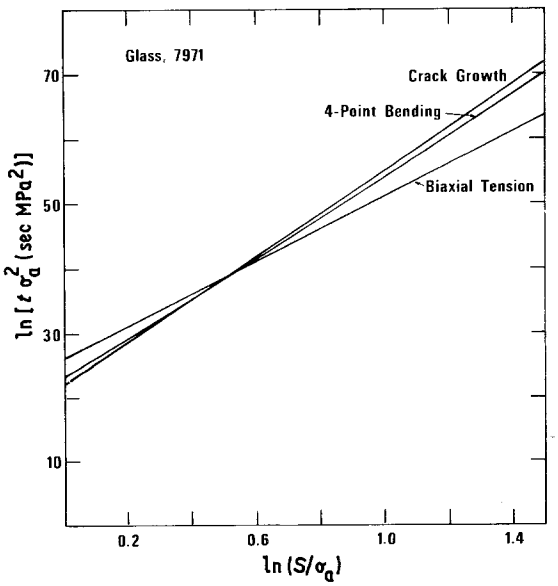

Figure 6 Failure prediction diagram comparing fracture mechanics and strength data for ultra-low-expansion glass.

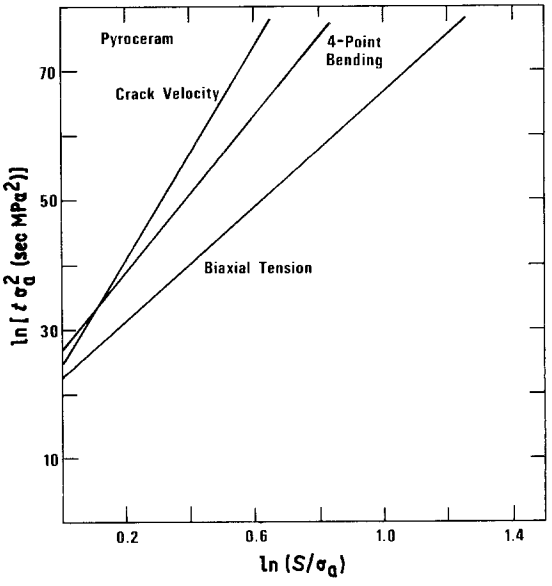

Figure 7 Failure prediction diagram comparing fracture mechanics and strength data for Pyroceram glass-ceramic.

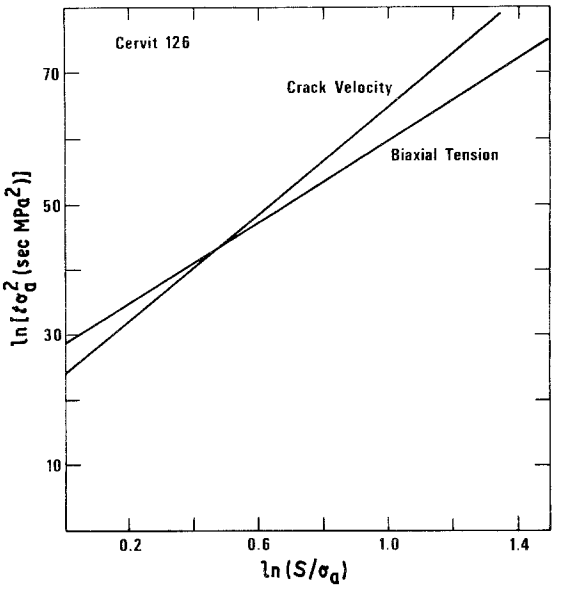

Figure 8 Failure prediction diagram comparing fracture mechanics and strength data for Cervit 126 glass-ceramic.

data obtained on the 18 μm aluminium oxide, and perhaps for the Cervit 126. For the other materials, the predicted lifetimes of a component under stress appear to depend on the test technique used to characterize the fatigue behaviour of the ceramic; statistical methods can be used to confirm this conclusion.

Because the values of the linear regression coefficient n were determined by direct analysis of experimental data, a Student t-test may be used to test the significance of the differences in the slopes shown in Figs 6 to 10. Table V presents the results of a Student t-test applied to the slopes, n, of the experimental data. The t-test confirms our intuitive feeling that differences in the slopes of the data for glass were not significant, regardless of the test used to determine n. The values of t in Table V also suggest that values of the slope obtained by the four-point bend test and the biaxial tension test did not differ significantly for any of the materials. By contrast, significant differences in

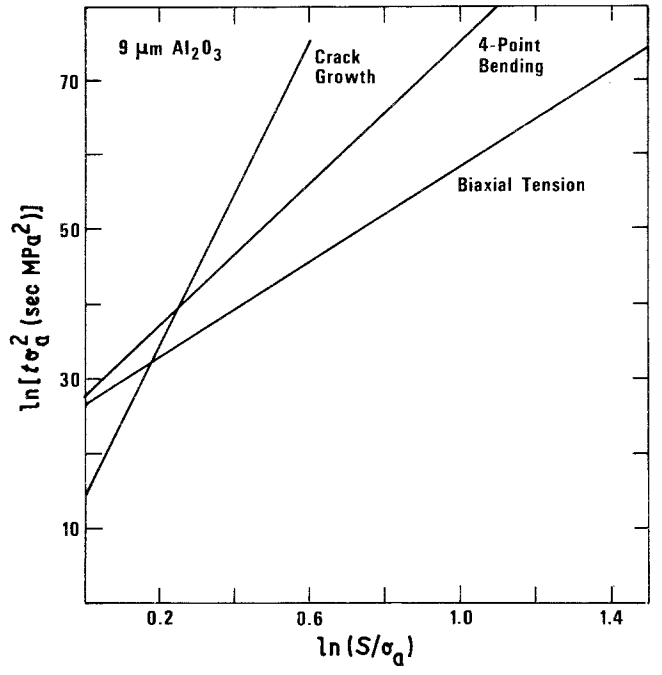

Figure 9 Failure prediction diagram comparing fracture mechanics and strength data for 9 μm grain-size aluminium oxide.

TABLE V Student t-test applied to the slope ($n - 2$) of the curves shown in Figs 6 to 10. Values of t that are significant at the 95 % probability level (two-sided probability) are underlined

Material	Four-point bend against biaxial tension	Four-point bend against crack velocity	Biaxial tension against crack velocity
Ultra-low-expansion glass (C7971)	1.59	0.649	1.99
Pyroceram glass-ceramic	1.08	1.38	3.98
Cervit 126 glass-ceramic	-	-	0.92
9 μm Al_2O_3	1.31	2.47	3.72
18 μm Al_2O_3	1.11	3.29	3.45

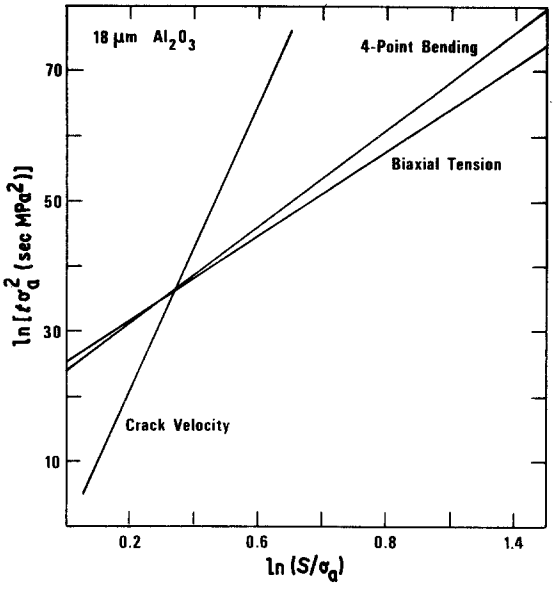

Figure 10 Failure prediction diagram comparing fracture mechanics and strength data for 18 μm grain-size aluminium oxide.

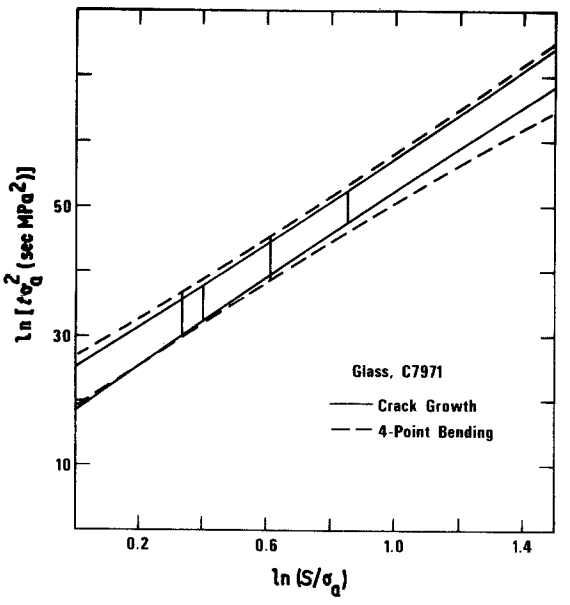

Figure 11 Ninety-five per cent confidence bands for two of the failure prediction lines shown in Fig. 6. Overlap of the confidence bands within the region of the data is taken as evidence that the intercepts of the two sets of data do not differ significantly. The range of S/σ_a corresponding to the range of the experimental data is indicated by the vertical lines in the figure.

slope, n, were obtained when the crack velocity method of evaluating n was compared with either of the two strength methods. A comparison of the crack-velocity technique with the biaxial tension technique indicates a significant difference in n for the Pyroceram, the 9 μm aluminium oxide and the 18 μm aluminium oxide. A comparison of the crack velocity technique with the four-point bend technique indicates a significant difference in n for the 18 μm aluminium oxide and the 9 μm aluminium oxide, but not for the Pyroceram.

A statistical comparison of the intercept of the curves presented in Figs 6 to 10 is not straightforward because $\ln B$ is a derived quantity not obtained by a direct linear regression analysis of experimental data. A qualitative comparison of the intercepts of these curves for different techniques of measurement can be obtained, however, by comparing the confidence bands associated with the curves in Figs 6 to 10. A comparison of this type is shown in Figs 11 and 12. The confidence bands are nearly hyperbolic curves that lie on each side of the central line (not included in Figs 11 and 12) predicted from Equation 7. The region of minimum approach to the central line represents that portion of the line for which confidence in the expected value of $\ln (t\sigma_a^2)$ is greatest. This region of the curve also corresponds to the range of $\ln \dot{\sigma}$ or $\ln K_I$ on the stressing-rate or crack-velocity curves over which the data were collected.* Two techniques of determining $\ln B$ can be compared by examining the confidence bands within the region of closest approach to the central line. Overlap of the confidence bands within this region suggests that the intercepts of the two sets of data do not differ significantly.

The method of comparison just described was applied to the sets of data in Table V that did not differ significantly in slope. The following sets of data were found to have intercepts that also did not differ significantly: the glass and Cervit 126 for all test techniques; the 18 μm aluminium oxide for the two stressing-rate techniques; and the Pyroceram for the four-point bend strength technique and the crack-velocity technique. By contrast, the 9 μm aluminium oxide and Pyroceram data, both obtained by the two stressing-rate

*This last point can be confirmed by examination of the equations used for the calculation of var $(\ln t\sigma_a^2)$; see the Appendix.

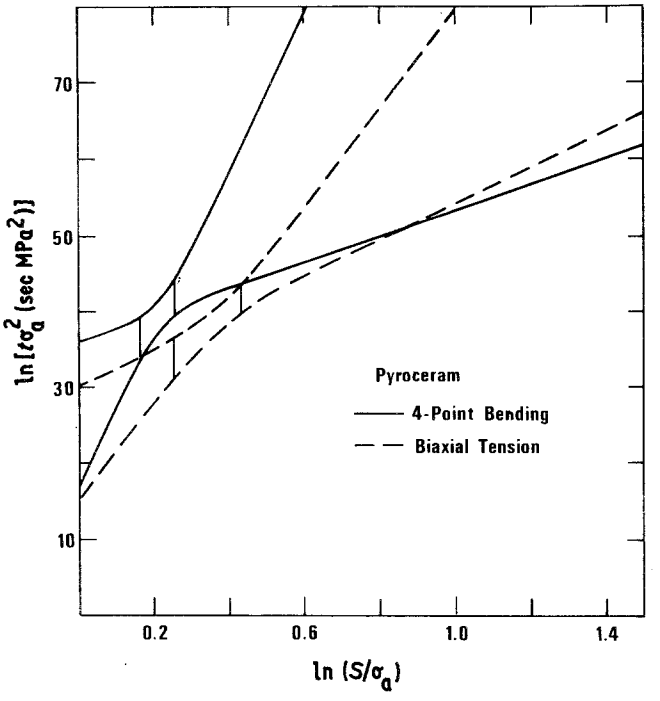

Figure 12 Ninety-five per cent confidence bands for two of the failure prediction lines shown in Fig. 7. The lack of overlap of the confidence bands within the region of the data is taken as evidence that the intercepts of the two sets of data differ significantly. The range of S/σ_a that corresponds to the range of the experimental data is indicated by the vertical lines in the figure.

techniques, had intercepts that differed significantly.

5. Discussion of results

5.1. Crack propagation parameter, n

The materials used in the present investigation have also been used by other investigators to study the static fatigue of ceramic materials. Since values of n were reported in all of these studies, a comparison of our data with those of other investigators (Table VI) can be made on the basis of the crack propagation parameter, n. For convenience of comparison, Table VI has been divided into three groups of data: Group 1 refers to data collected on the same lots of materials using measurement techniques that were essentially identical to those used in our study; Group 2 refers to materials that were similar, but not identical in structure and composition to those used in the present study; Group 3 refers to materials or test techniques that differed substantially from those used in the present study. As will be seen, some of the data agreed very well with those collected in our study, whereas other data differed substantially from our own.

The data from Table VI that compared best with our own were those collected on the same lots of material used in the present study (Group 1). A comparison of these data with our own indicates that the values of n reported in Table VI fall within a standard deviation of the values given in Table I for the same measurement technique. This comparison suggests that the data from the first group of Table VI are statistically indistinguishable from those obtained in the present paper. Since material variability is not a factor in this interlaboratory comparison, we conclude that the techniques used for the characterization of static fatigue can be duplicated at different laboratories to obtain consistant values of n for a given material.

With the exception of the Pyroceram 9606 data collected by Koepke [16], the data from Table VI, Group 2, differs substantially from those obtained in the present paper.* Part of this difference is accounted for by small differences in microstructure and composition of the materials studied. The effect of microstructure is clearly demonstrated by the work of Ritter and Cavanaugh [26]. Using four-point bending, the stressing technique was employed by these authors to obtain measurements of n on a Cervit 126-type glass-ceramic. As shown in Table VI, Ritter and Cavanaugh observed a dramatic increase in the

*The material studied by Koepke was supplied to him by us, but was from a different billet than that reported here.

TABLE VI Summary of static fatigue data. All tests were conducted in water

Material	n	Test	Comments	Reference
Group 1				
Cervit 126	36.7	Double torsion		Koepke *et al.* [24]
9 μm aluminum oxide	90	Double torsion		Koepke [16]
Group 2				
Pyroceram 9606	85	Double torsion		Koepke [16]
Pyroceram 9606	55	Double torsion		Bansal and Duckworth [25]
Cervit 126	52.3	Four-point bend	0.5 μm Keatite	Ritter and Cavanaugh [26]
Cervit 126	180.6	Four-point bend	1.5 μm Keatite	Ritter and Cavanaugh [26]
Aluminium oxide	35.7	Double torsion	Non-commercial sintered material	Ferber and Brown [27]
Aluminium oxide	52.0	Double torsion	Lucolox	Evans *et al.* [28]
Aluminum oxide	42	Double torsion	Alsimag 614	Bansal and Duckworth [25]
Aluminium oxide	37.4	Four-point bend	Electronic substrate	Ritter and Humenik [14]
Group 3				
Aluminum oxide	45.9	Double cantilever beam	Luncolox H.S. 6–8 μm grain size	Freiman *et al.* [30]
Aluminium oxide	30.6	Double cantilever beam	Lucolox H.S. After annealing, 30–40 μm grain size	Freiman *et al.* [30]
Aluminium oxide	56 to 158	Double torsion	Alumina refractories	Adams *et al.* [29]
Aluminium oxide	10.3 to 43.9	Stressing rate (Three-point bending)	Alumina refractories	Adams *et al.* [29]
Pyroceram 9606	89	Four-point bend	Specimens polished and indented	Cook *et al.* [31]

value of n, 52.3 to 180.6, as the grain size of the glass-ceramic increased from 0.5 μm to 1.5 μm. A much smaller difference in grain size would account for the lower value of n, 32.9, obtained in our study of Cervit 126.

Differences in microstructure and composition may also account for the values of n obtained for some of the aluminium oxide data shown in Table VI [25, 27]. The sintered material used by Ferber and Brown [27] contained approximately 6% porosity, whereas the material used by Bansal and Duckworth [25] was reported to have glass at the grain boundaries. Although effects of porosity and grain-boundary glass on crack growth have not yet been studied in great detail, it is possible that these microstructural effects account for the difference in the reported crack growth behaviour. Glass at the grain boundaries may be particularly important because of the susceptibility of glass to subcritical crack growth [1].

Minor differences in experimental technique may also account for some of the difference between our data and the data given in Table VI (Group 2). All double-torsion data shown in Table VI were collected by the relaxation procedure. This technique is particularly susceptible to spurious relaxation that can occur during the course of a measurement. These relaxations may result from mechanical relaxation of the test apparatus or from localized plastic deformation and fracture at the bearing surfaces of the test fixture. Relaxations of this sort will cause the

measured value of n to be less than the value of n obtained in the absence of spurious relaxations. The cause of these relaxations and methods of avoiding them have been discussed in some detail by Pletka *et al.* [17].

Group 3 of Table VI contains a summary of three sets of data, one set collected on dense aluminium oxide using the double-cantilever beam technique, another set collected on aluminium oxide refractory materials using the double-torsion technique and the final set collected on the same billet of Pyroceram used in the present studies, but with indentation cracks as fracture nuclei. The work by Adams *et al.* [29] on the refractories illustrates, in a dramatic way, the effect of microstructure on fatigue behaviour. In a study of 10 different commercial refractories that ranged in composition from 42 to 91% aluminium oxide, these authors showed that n varied from 56.1 to 157.8 when obtained by the double-torsion technique. By contrast, when n was determined by a constant stressing-rate technique, n varied from 10.3 to 43.9. The value of n obtained by the double-torsion technique was found to range from approximately three to six times the value obtained by the stressing-rate technique. The same sort of result was obtained in the present study for aluminium oxide, for which n obtained by the double-torsion technique was found to be approximately three times the value obtained by the stressing-rate techniques.

The data of Freiman *et al.* (Table VI) [30] suggests that if a constant driving-force technique is used instead of a relaxation technique, the measured value of n is reduced considerably. Freiman *et al.* [30] used the applied-moment, double-cantilever beam technique to measure crack growth in several grades of aluminium oxide. Two of the materials studied were fully-dense, Lucolox specimens (6 to 10 μm and approximately 50 μm grain size) that were similar to the specimens used in the present study. The low values of n obtained by Freiman *et al.* can be attributed to the fact that cracks were forced to propagate through regions of localized toughness by the constant driving force used in their experiments. Cracks were reported to have undergone periods of acceleration and deceleration even though the driving force for fracture remained constant. The crack velocities reported by Freiman *et al.* were determined by averaging the crack growth over relatively long distances of motion (approximately 0.5 mm) [32] in the test specimen. Therefore, the data represent a measure of the average resistance of the test material to crack growth. By contrast, when a relaxation technique is used to study crack growth, the driving force for fracture decreases as the crack grows longer, and there is a tendency for crack arrest by regions of high toughness. As discussed below, this tendency for crack arrest may explain the high values obtained for n by relaxation procedures.

The data collected by Cook *et al.* [31] demonstrate a significant effect of the mechanical condition of the surface on the apparent value of n obtained by constant stressing-rate techniques. In their study, Cook *et al.* introduced indentation cracks into four-point bend specimens that had been mechanically polished. The cracks served as fracture nuclei during strength measurements. As can be shown from a Student t-test, the value of n, 89, obtained by these authors differed significantly from those reported in Table III. The fact that the same billet of material was used in both studies suggests that differences in n values can be attributed to differences in surface condition. As discussed below, Cook *et al.* attribute these differences to the presence of residual stresses in the surface of the specimens. The presence of these stresses in the vicinity of crack nuclei will effect the motion of these cracks and hence the stressing-rate behaviour of the test specimens.

5.2. The effect of microstructure and test technique on n

An analysis of the experimental results of this paper (Section 3) indicates that of the five materials tested only the glass and the Cervit 126 gave values of n and $\ln B$ that were independent of the test technique. Considering the fact that the glass and the Cervit 126 are homogeneous and have fine microstructures compared to the other three materials, these results suggest that the values obtained for $\ln B$ and n may depend in some way on the microstructure of the materials tested. Hence, it seems useful to discuss the effect of microstructural parameters on crack growth, and to explore the possibility that microstructural effects account for the relatively high value of n obtained on Pyroceram and aluminium oxide when n is measured by the double-torsion technique. The arguments in this section will be developed in two stages: one relating to the crack growth experiments; the other relating to the stressing-rate experiments.

A number of recent publications have reported the fact that the fracture resistance of some ceramic materials increases as the size of the pre-existing crack is increased by subcritical crack growth. Studies by Hübner and Jillek [33] on aluminium oxide (18 μm grain size, 4% porosity) using single-edge-notched, four-point bend specimens indicate an increase in K_{IC} from 2.7 to 4.6 MPa $m^{1/2}$ as the crack length changed by only 1 mm. Microscopic evidence was presented by these authors to show that this finding was largely the result of crack branching and the formation of multiple cracks. Pratt [34], who used double-cantilever beam specimens, showed the same sort of increase in K_{IC} if measurements of K_{IC} were made after subcritical crack growth occurred in the test specimens. He also attributed the increase in K_{IC} to an increase in the amount of multiple cracking in the test specimens. Bansal and Duckworth [35], in a study of the strength of two different grades of aluminium oxide, also obtained support for the observations of Hübner and Jillek. Hence, there is a body of evidence in the literature that supports the idea that the fracture resistance of ceramics can increase during crack propagation.

The studies of Freiman *et al.* [30] cast a somewhat different light on the effect of microstructure on crack propagation. These authors report a cyclic behaviour to the crack velocity for cracks that were subjected to a constant applied-stress intensity factor, which suggests that the resistance of the material to fracture varies in a cyclic manner as the crack gets longer. To be consistent with the results of Hübner and Jillek, this variation in resistance to fracture would have to be determined by a rise and decay in the extent of microcracking as the crack grows longer. Since the extent of microcracking is probably determined by the local microstructure at the crack tip, variations in resistance to fracture are ultimately determined by variations in the crack tip microstructure.

Pletka *et al.* [17] have obtained data that support the findings of Freiman *et al.* Using the double-torsion technique, these authors measured the rate of crack growth on specimens subjected to a constant rate of displacement. Normally, when this test method is applied to a homogeneous material, such as glass, a smooth, constant-load plateau is obtained when the rate of machine displacement is just compensated for by the rate of relaxation of the specimen due to crack motion. The crack velocity and the applied stress intensity are then uniquely determined by the magnitude of the load corresponding to the load plateau. In the experiments conducted by Pletka *et al.* [17] the plateau was irregular and the applied load could not be determined uniquely. As with the data collected by Freiman *et al.* [30], this data can be understood by recognizing that the resistance of the solid to crack motion varied as the crack propagated. Variations of the load during a crack growth experiment would then correspond to local variations of the resistance of the material to crack growth.

The fracture studies just discussed can serve as a basis for understanding the dependence of n on test technique. In a qualitative way, the fracture studies indicate the existence of a spacial variation in the resistance of heterogeneous solids to fracture. This spacial variation in fracture resistance can, in principle, bias experimental measurements of crack growth parameters, so that the parameters depend on the experimental technique used for their determination. When fracture mechanics techniques are used to determine crack growth parameters, one might expect the overall behaviour of the crack to be determined by regions of high resistance to crack growth. Cracks tend to be slowed by regions of high resistance, and hence, most of the time for crack propagation is spent trying to overcome these regions.

When stress relaxation techniques are used to measure crack growth parameters, variations in the local resistance of the material to fracture can bias the slope of the crack growth curve because of the manner in which the data are collected. The data points on a crack velocity curve are not truly independent, in the sense that the data points are of necessity taken in sequence from the highest to the lowest value of K_I as the driving force for fracture decreases during the relaxation process. Because the data points are not independent, structural variations in the material are bound to affect large numbers of data points from each relaxation run, and hence, will effect the slope and shape of the entire curve. If, as has already been suggested, the crack spends most of its time trying to overcome regions of high fracture resistance, the slope of the crack growth curve is expected to be biased towards high values of n. The biasing of n arises because an incremental increase in the resistance to crack growth causes the velocity to decrease by a larger increment than would be obtained if the resistance to crack

motion remained constant as the crack grew longer. This explanation for the high value of n depends somewhat on the state of the crack and its location at the start of the relaxation experiment. If the crack were just entering a region of easy crack growth, then crack acceleration, or a low value of n would be expected in the course of the relaxation experiment. Local accelerations of this type have been reported earlier [21] and are illustrated in Fig. 1 for the Pyroceram data. Furthermore, low values of n are frequently encountered in the initial stages of a relaxation experiment, Fig. 2, suggesting that easy regions of crack growth are more frequently encountered at high crack velocities. These observations lend support to the mechanism of crack growth proposed herein.

The magnitude of change in fracture resistance of the material can be small and yet still account for the results observed in the present paper. This can be demonstrated by comparing the data in Fig. 2 for which $n \simeq 100$ with data reported by Freiman *et al.* for which $n \simeq 45.9$. For the sake of discussion, it will be argued that the lower value of $n = 45.9$ is an unbiased representation of the true average fracture resistance of aluminium oxide. The higher value, $n \simeq 100$, will be assumed to be representative of data for which microstructural effects have biased the value of n. For the range of crack velocities (10^{-4} to 10^{-8} m sec^{-1}) used by Freiman *et al.*, the change in K_I was approximately 0.6 MPa m$^{1/2}$. The change in K_I for the higher value of n would be approximately 0.3 MP a m$^{1/2}$ for the same velocity range. The difference between these two values, 0.3 MPa m$^{1/2}$, represents the increase in fracture resistance of the material during the course of the relaxation experiment that would be required for the higher value of n. Changes in K_I of this magnitude are reasonable considering the fact that a much larger effect of crack growth on K_{IC} has been reported for aluminium oxide [33, 34]. A change in K_I of this magnitude is also consistent with variations in loads obtained when crack velocity curves are determined on double-torsion specimens using the constant stressing-rate technique [17]. Hence, it is our opinion that the data in the literature support the hypothesis that the high values of n obtained by stress relaxation procedures can be attributed to an increase in the fracture toughness of the material during the course of the relaxation measurement.

The microstructural effects just discussed are likely to bias crack growth parameters differently when these parameters are determined on strength specimens by stressing-rate techniques. The surfaces of ceramic materials contain large numbers of flaws that vary in size and location. Although the largest flaws are generally the most likely to propagate to failure in the course of a strength test, the location of the flaw in the material is almost as important as its size in the determination of material strength. Flaws that are located in regions of the material that have a low resistance to crack propagation will tend to be the first to propagate to failure. Hence, the stressing-rate technique of determining n is biased by regions of the solid that exhibit a low resistance to crack propagation. The stressing-rate technique is less likely to be influenced by interactions of cracks with fracture resistant portions of the solid. If one of the cracks were stopped, or slowed by the microstructure, a second crack in a less resistant portion of the solid would surpass the first in size and would become the source of failure. Because of this behaviour, material-induced biasing of the experimental results will be different for the stress relaxation and the constant stressing-rate techniques. The values of n determined by the stressing-rate technique is likely to be less than that determined by the stress relaxation technique.

The concepts presented in the preceeding paragraph are supported in part by the work of Mendiratta and Petrovic [36]. These authors studied the growth of individual flaws that were introduced into hot-pressed silicon nitride (HS130) by Knoop indentation. Studies were conducted in a vacuum at 1300° C so that crack growth was the result of creep–fracture. These authors found that cracks that were originally of equal size tended to grow at different rates so that after a period of time the cracks were not the same size. Cracks with an initial surface length of 0.167 mm were found to range in size from approximately 1.1 mm to approximately 2.7 mm after 19 min exposure at a stress of 206 MPa. These results were attributed to microstructural heterogeneities in the test material. Since the results reported by Mendiratta and Petrovic were obtained at elevated temperatures there may be some reason to believe that their results are restricted to the material and test condition used by these authors. However, it is the opinion of the present authors that the effect is probably much more general, and therefore

applies also to strength measurements on brittle materials at low temperatures.

A second explanation for the relatively low value of n obtained from stressing-rate experiments has been presented recently by Marshall and Lawn [37]. Most surface flaws in ceramic materials are formed as the result of contact loads that occur during the machining and finishing of these materials. Contact loads introduce cracks into the surface of the solid which act as the primary sources of failure in ceramic materials. Since contact loads also deform the solid plastically at the point of crack initiation, residual stresses caused by the plastic deformation tend to force the cracks open, resulting in stresses at the tips of these surface cracks. During a strength measurement, the residual stresses add to the stresses from the applied load, and thus modify the apparent static fatigue behaviour of the material. In their study on soda-lime–silica glass, Marshall and Lawn showed that the value of n (13.2) for indented specimens tested in four-point bending was less than the range of values obtained by crack growth measurements (16 to 19). In a more recent study of this phenomenom, Cook *et al.* [31] have shown that crack-growth and strength data obtained on Pyroceram can also be reconciled by considerations of surface stresses induced by machining. Hence, an effect such as this undoubtedly plays a role in determining the value of n obtained by stressing-rate procedures, and therefore offers an alternative explanation for the fact that the value of n is low when determined by these procedures. Clearly, additional research is needed to develop a full understanding of the effect of measurement technique and microstructure on the value of n.

5.3. Prediction of component lifetime

Methods of design for ceramic materials are based on the premise that failure originates from pre-existing flaws that undergo subcritical crack growth. The rate of growth, the applied forces and the crack length are assumed to be functionally related. In principle, the parameters that determine this relationship can be evaluated experimentally so that the basic assumptions of the theory can be checked. In this section of the paper, the data presented earlier will be used to make lifetime predictions for a hypothetical application for which the applied stresses are held constant. As will become apparent, large differences in the predicted lifetime occur primarily as a result of differences in the experimental value of the crack propagation parameter n. Effects of measurement error are also discussed, and are shown to be a source of uncertainty in the prediction of lifetime.

Lifetime predictions can be made by the use of Equation 7 in a slightly modified form:

$$\ln t = \ln B + (n-2)\ln S - n \ln \sigma_a. \quad (9)$$

The constants required for this equation appear in Tables I to IV. Estimates of error in the expected failure time, t, were obtained by the methods outlined in [5] and [39] (see the Appendix for a summary of these methods). Fig. 13 illustrates the type of relation obtained between the three variables (t, S and σ_a) of Equation 9. In Fig. 13, $\ln t$ and $\ln \sigma_a$ are used as the ordinate and abscissa, whereas the lines on the diagram represent the relation between these two variables for selected values of inert strength, S. For each value of S, the central line is calculated from Equation 9,

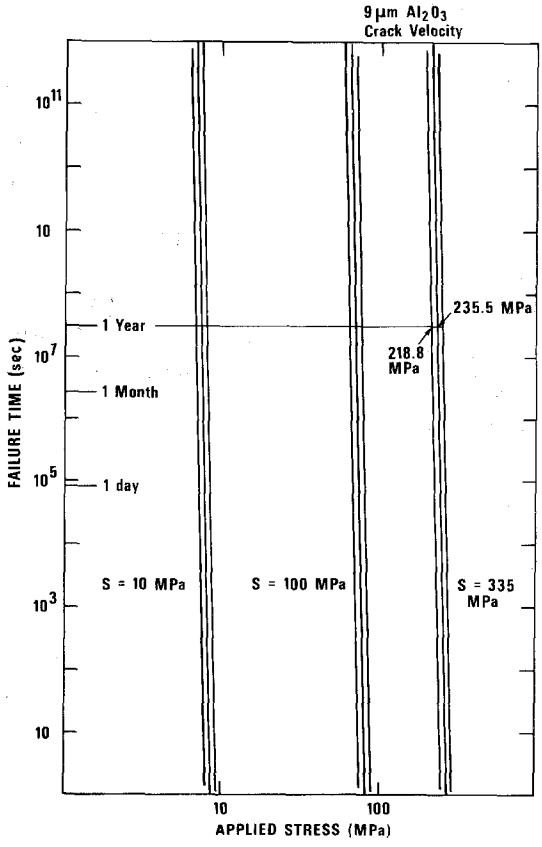

Figure 13 Lifetime prediction curves obtained for 9 μm aluminium oxide. The curves were calculated from crack propagation data. Error bands represent 95% confidence limits for the central lines.

TABLE VII Predicted service stress (MPa) for a one-year lifetime, based on median estimate of the prediction time

Material	Inert strength (MPa)	Crack velocity	Technique	
			Biaxial tension	Four-point bending
Ultra-low-expansion glass (C7971)	100	40.3	35.5	39.8
Pyroceram glass-ceramic	160	112	81.3	105
Cervit 126 glass-ceramic	100	53.7	46.8	–
9 μm Al_2O_3	335	235.5	140.6	151.4
18 μm Al_2O_3	250	153.1	103.0	112

whereas the outer curves, which represent 95% confidence limits for the estimation of $\ln t$, are determined by methods discussed in the Appendix. Because the slope of the central line is given by $-n$, the prediction lifetime is very sensitive to experimental evaluation of this parameter: the lower the value of n, the larger the relative reduction in strength as a result of static fatigue.

The widths of the error bands shown in Fig. 13 are sensitive to the accuracy with which the constants of Equation 9 are determined. The estimated error in the mean failure time can be substantial. In Fig. 13 for example, a one-year estimate of lifetime for an applied stress of 235.5 MPa and an initial strength of 335 MPa could be in error by as much as approximately three orders of magnitude: failure could occur in a time as short as approximately 4 days or as long as 200 years. For practical applications, this magnitude of error is not as serious as it might first appear, because of the large slope ($n \simeq 100$) of the curves shown in Fig. 13. Small reductions in applied stress result in large increases in the survival probability [5]. Referring again to Fig 13, a reduction in applied load from approximately 235.5 MPa to approximately 218.8 MPa (the lower bound of the confidence band) reduces the chance of failure in a period of less than one year to 2.5%. Additional reductions in the applied load would decrease the chance of failure even further. In general, this type of logic holds for all of the materials studied. By basing the lifetime prediction on the lower bound of the confidence band, a high assurance of lifetime can be achieved with only marginal reduction of load carrying capability [5].

In Tables VII and VIII comparisons of predicted lifetime are presented for each of the techniques used in this study. For each material and test technique, a graph such as that shown in Fig. 13 was obtained. The applied stress required for a lifetime of one year was then calculated for the line representing the mean estimate of lifetime, and for the curve representing the lower bound of the 95% confidence band. The initial strength for each material was estimated as approximately three standard deviations below the mean breaking

TABLE VIII Predicted service stress (MPa) for one-year lifetime, based on lower probability band of the predicted line

Material	Inert strength (MPa)	Crack velocity	Technique	
			Biaxial tension	Four-point bending
Ultra-low-expansion glass (C7971)	100	37.6	25.1	34.7
Pyroceram glass-ceramic	160	105	60.3	63.1
Cervit 126 glass-ceramic	100	44.7	41.7	–
9 μm Al_2O_3	335	218.8	128.8	77.6
18 μm Al_2O_3	250	144.5	79.4	107

stress given in Table II. This estimate of the initial strength is considered to be a realistic level of practical load for each of the materials studied.

Table VII presents an estimate of the allowed service stress for a lifetime of one year, based on a mean estimate of lifetime. Because of subcritical crack growth, substantial decreases in the service stress (below the initial strength) are required for all materials studied. The largest decrease in allowable stress occurs for materials that exhibit the smallest values of n, indicating the importance of this parameter to the calculated lifetime. Glass, tested by the biaxial tension technique ($n = 26$) is predicted to exhibit a 64.5% loss in strength over a one year period, whereas the Pyroceram ($n = 83.5$) or the 9 μm aluminium oxide ($n = 104$) tested by the crack velocity technique is predicted to suffer a loss of only 30% in strength during the same period. This same dependence of strength on test techniques is noted for each of the materials studied. In general, lower allowable service stresses are calculated when data from the biaxial tensile test are used for estimates of lifetime because the lowest values of n were obtained by this technique.

As illustrated in Table VIII, sizable reductions in the allowable applied stress are required for design purposes when errors of measurement are factored into the selection of the applied stress. The magnitude of the reduction depends on the accuracy of the data used for the prediction of lifetime. When the original fatigue data are very accurate, a negligible reduction in applied stress is required to account for experimental error. Thus, a reduction in stress level of only 2.7 MPa (approximately 7%) would be needed to account for experimental error for the ultra-low expansion glass analysed by the crack velocity technique. By contrast, when strength data are subject to considerable experimental scatter, as they are for Pyroceram tested in four-point bending, large reductions in applied stress are required to account for measurements errors. For the Pyroceram, a reduction of the applied stress from 105 MPa to 63.1 MPa (approximately 40%) is necessary to account for errors of measurement. Needless to say, errors of measurement must be minimized to attain accurate predictions of lifetime.

Assuming that measurement errors can be reduced to an acceptable minimum, the lowest of the predicted service stress would normally be used for the greatest assurance of design lifetime. For this reason, the predicted service stresses obtained by the stressing-rate techniques would be preferred over those obtained by the crack velocity technique because they are lower.

A second reason for the selection of stressing-rate data over crack growth data for purposes of lifetime prediction has to do with the effect of microstructure on crack propagation. As noted earlier, experimental data obtained by the two techniques are biased quite differently by the microstructure and hence lead to considerable differences in predicted lifetime when there are interactions between the microstructure and the moving cracks. Because of this possibility, data from test techniques that relate most closely to the actual application should be used for the prediction of lifetime. For most applications, the lifetime of ceramics is limited by the critical condition of initial instability of small cracks that are normally present in ceramic materials. Once these cracks begin to move they are subject to a continually increasing driving force which reduces the likelihood of arrest before failure. Since they duplicate the conditions that occur in practice, stressing-rate techniques are more appropriate for the prediction of component lifetime for most applications. In those cases where the interest is also in crack arrest (thermal shock, erosion etc.) measurement of static fatigue parameters by crack growth techniques (specifically relaxation techniques) may also be appropriate for the prediction of lifetime. Where crack growth and crack arrest are considered important, both types of data would have to be used for design.

6. Summary

The primary objective of this paper was to examine the premise that the crack growth parameters, n and B, which are used for structural design, depend only on material composition and microstructure. To test this premise, a test matrix of five materials and three test techniques were used to determine these crack growth parameters. The test techniques were: (a) double-torsion technique, relaxation method; (b) stressing-rate technique, four-point bend specimens; (c) stressing-rate technique, biaxial tension specimens. Two of the materials tested (ultra-low-expansion glass, C7971; Cervit 126) gave results that were independent of test technique. The other three materials (Pyroceram 9609, 9 μm Al_2O_3 and 18 μm Al_2O_3) gave results that depended on test technique.

The results were explained on the basis of the

microstructures of the materials tested. The microstructures of the Pyroceram and the two aluminium oxides were considerably coarser than those of the other two materials. Hence, it was hypothesized for these three materials that interactions between the crack tip and the microstructure explained the lack of experimental consistency for the test techniques. The occurance of multiple fracture at the tip of the moving crack, and the intersection of the crack tip with particularly tough regions of the material was used to explain the relatively large values of the parameter n obtained by relaxation measurements. This explanation is consistent with observations of multiple fracture in aluminum oxide and with observations of cyclic acceleration and deceleration of cracks in aluminum oxide that are subject to a constant driving force. Microstructural interactions are not as important in stressing-rate experiments because of the multiplicity of potential fracture sites in the surfaces of specimens normally used in these experiments.

From a practical point of view, it was suggested that for most applications, stressing-rate experiments should be used to determine the crack propagation parameters n and B. This suggestion was made because of the necessity of a conservative approach in the prediction of lifetime, and because the flaws that cause failure in stressing-rate experiments closely duplicate those that cause failure in most engineering situations. In situations where crack arrest is important (i.e. thermal shock, erosion, etc.) crack growth parameters obtained by stress relaxation procedures may also be appropriate.

Acknowledgement

One of the authors (BJP) gratefully acknowledges the National Research Council for support as a Post Doctoral Research Associate at the National Bureau of Standards, where much of this work was carried out.

Appendix: Method used to establish confidence limits for $\ln (t^2 \sigma_a)$

Confidence limits for Equation 7 were determined from estimates of the variance of $\ln (t\sigma_a^2)$ and the number of degrees of freedom in each experiment. Using the procedures outlined in [5] and [38], the following equation is obtained for the estimate of the variance of $\ln (t\sigma_a^2)$ for the crack propagation data:

$$\begin{aligned}\text{var}(\ln t\sigma_a^2) &= (n-2)^2 \text{ var}(\langle \ln K_{IC} \rangle) \\ &+ \text{var}(\langle \ln v_0 \rangle) + [\langle \ln K_{IC}/K_0 \rangle - \ln (S/\sigma_a) \\ &+ (n-2)^{-1}]^2 \text{ var}(\langle n \rangle) + 2[\langle \ln K_{IC}/K_0 \rangle \\ &- \ln (S/\sigma_a) + (n-2)^{-1}] \text{ cov}(\langle n \rangle, \langle \ln v_0 \rangle) \end{aligned} \quad \text{(A1)}$$

where var $(\langle \ln v_0 \rangle)$, var $(\langle n \rangle)$ and cov $(\langle n \rangle, \ln \langle v_0 \rangle)$ are given by the following equations:

$$\text{var}(\langle n \rangle) = \left[\sum_{i=1}^{N} (n_i - \langle n \rangle)^2 \right] / N(N-1), \quad \text{(A2)}$$

$$\text{var}(\langle \ln v_0 \rangle) = \left[\sum_{i=1}^{N} (\ln v_{0i} - \langle \ln v_0 \rangle)^2 \right] / N(N-1) \quad \text{(A3)}$$

and

$$\text{cov}(\langle n \rangle, \langle \ln v_0 \rangle) = \left[\sum_{i=1}^{N} (n_i - \langle n \rangle)(\ln v_{0i} - \langle \ln v_0 \rangle) \right] / N(N-1), \quad \text{(A4)}$$

TABLE AI Summary of data obtained by fracture mechanics techniques

Parameter	Ultra-low expansion glass (C7971)	Pyroceram glass-ceramic (C9606)	Cervit 126 glass-ceramic	9 μm Al_2O_3	18 μm Al_2O_3
$\ln K_0$	0	0	0	0	0
$\langle n \rangle$	35.0	83.5	45.5	104.1	111.3
$\langle \ln v_0 \rangle$	−470	−1224	−625	−1583	−1724
$\ln K_{IC}$	13.4588	14.6571	13.7102	15.2857	15.7339
var $(\langle \ln K_{IC} \rangle)$	6.072×10^{-4}	5.093×10^{-4}	2.316×10^{-3}	6.345×10^{-4}	3.673×10^{-4}
var $(\langle \ln v_0 \rangle)$	118.986	1556.230	3158.489	8179.840	18226.782
var $(\langle n \rangle)$	0.7496	7.634	17.253	35.1592	80.270
cov $(\langle n \rangle, \langle \ln v_0 \rangle)$	−9.4264	−108.894	−233.43	−535.972	−1209.487
Degrees of freedom					
K_{IC} data	3	3	2	3	5
v–K data	3	4	4	8	4

TABLE AII Summary of data obtained by strength measurement techniques (biaxial tension)

Parameter	Ultra-low expansion glass (C7971)	Pyroceram glass-ceramic (C9606)	Cervit 126 glass-ceramic	9 μm Al_2O_3	18 μm Al_2O_3
$\ln \dot{\sigma}_0$	0	0	0	0	0
n	26.9	46.3	32.9	33.8	34.5
$\ln \sigma_{f_0}$	18.238	18.440	17.954	18.916	18.668
$\ln S_i$	19.254	19.092	18.657	19.757	19.508
var ($\langle \ln S_i \rangle$)	1.037×10^{-3}	2.527×10^{-4}	1.4157×10^{-4}	2.1525×10^{-4}	2.769×10^{-4}
var ($\ln \sigma_{f_0}$)	40.96×10^{-4}	16.81×10^{-4}	8.410×10^{-4}	4.41×10^{-4}	24.01×10^{-4}
var (n)	12.96	40.96	5.29	2.89	16.81
$\langle \ln \dot{\sigma} \rangle$	13.5144	13.9639	13.6877	14.7594	14.5527
Degrees of freedom					
$\ln S_i$	29	14	7	8	9
Stressing-rate data	3	3	3	3	3

where N represents the total number of determinations made for n and $\ln \nu_0$ on each material, $\langle \ln K_{IC}/K_0 \rangle$ is the mean value of $\ln(K_{IC}/K_0)$, and var ($\langle \ln K_{IC} \rangle$) is the variance of the mean value of $\ln K_{IC}$.

For the strength data, the variance of $\ln (t\sigma_a^2)$ can be expressed directly in terms of stressing-rate parameters. The fracture stress, σ_f, of a set of laboratory specimens, measured as a function of the stressing-rate, $\dot{\sigma}$, is normally represented by the following empirical equation:

$$\ln \sigma_f = \ln \sigma_{f0} + M \ln (\dot{\sigma}/\dot{\sigma}_0), \quad \text{(A5)}$$

where $\ln \sigma_{f0}$ and M are constants determined by a linear regression analysis of the stressing-rate data, and σ_0 is an arbitrary normalization constant for the stressing-rate. By comparing Equation A5 with Equation 6 it can be shown that:

$$M = 1/(n+1) \quad \text{(A6)}$$

$$\ln B = (n+1) \ln \sigma_{f0} - (n-2) \langle \ln S_i \rangle - \ln (n+1) - \ln \dot{\sigma}_0, \quad \text{(A7)}$$

where $\langle \ln S_i \rangle$ is the mean value of the strength of a set of laboratory specimens measured in an inert environment. From Equation 7 and Equation A7 it follows that:

$$\ln (t\sigma_a^2) = (n+1) \ln \sigma_{f0} - (n-2) \langle \ln S_i \rangle - \ln (n+1) - \ln \dot{\sigma}_0 + (n-2) \ln (S/\sigma_a). \quad \text{(A8)}$$

Consequently, the variance of $\ln (t\sigma_a^2)$ is given by:

$$\text{var} (\ln t\sigma_a^2) = [\ln \sigma_{f0} - \langle \ln S_i \rangle - (n+1)^{-1} + \ln (S/\sigma_a)]^2 \text{ var} (n) + 2 [\ln \sigma_{f0} - \langle \ln S_i \rangle - (n+1)^{-1} + \ln (S/\sigma_a)] (n+1) \text{ cov} (n, \ln \sigma_{f0}) + (n+1)^2 \text{ var} (\ln \sigma_{f0}) + (n-2)^2 \text{ var} (\langle \ln S_i \rangle). \quad \text{(A9)}$$

TABLE AIII Summary of data obtained by strength measurement techniques (four-point bending)

Parameter	Ultra-low expansion glass (C7971)	Pyroceram glass-ceramic (C9606)	9 μm Al_2O_3	18 μm Al_2O_3
$\ln \dot{\sigma}_0$	0	0	0	0
n	33.3	62.5	49.3	39.2
$\ln \sigma_{f_0}$	17.469	18.893	19.130	18.678
$\ln S_i$	18.299	19.322	19.676	19.452
var ($\langle \ln S_i \rangle$)	2.44×10^{-3}	1.73×10^{-4}	2.8×10^{-4}	3.26×10^{-4}
var ($\ln \sigma_{f_0}$)	4×10^{-4}	24×10^{-4}	42.3×10^{-4}	0.64×10^{-4}
var (n)	3.24	184.96	136.89	0.81
$\langle \ln \dot{\sigma} \rangle$	12.425	14.320	13.612	14.023
Degrees of freedom				
$\ln S_i$	11	9	9	9
Stressing-rate data	3	5	3	3

Following the procedure outlined in [38] it can be shown that

$$\text{cov}\,(n, \ln \sigma_{f0}) = [\langle \ln \dot{\sigma} \rangle - \ln \dot{\sigma}_0]\ [1/(n+1)]^2\ \text{var}\,(n), \quad \text{(A10)}$$

where var $(n) = M^{-4}$ var (M). Although Equation A9 appears to be formidable, its application is straightforward once the appropriate experimental parameters have been obtained. It is worth noting that var $(\ln t\sigma_a^2)$ calculated from either Equation A1 or Equation A9 depends on the value selected for the variable S/σ_a. Consequently, the confidence limits for $\ln t\sigma_a^2$ will also depend on this variable. Finally, if σ_a is known without any error then var $(\ln t) = \text{var}\,(\ln t\sigma_a^2)$.

Once the number of degrees of freedom have been determined for each set of experiments, confidence limits for $\ln t\sigma_a^2$ can be determined. The number of degrees of freedom, ϕ, were estimated using the expression developed by Welsh [39]:

$$[\text{var}\,(\ln t\sigma_a^2)]^2/\phi = \sum_i [\text{var}\,(i)]^2/\phi_i, \quad \text{(A11)}$$

where var (i) is that part of var $(\ln t\sigma_a^2)$ due to variable i, and ϕ_i is the number of degrees of freedom used to determine var (i).

As an example of the application of Equation A11, consider the fracture mechanics data in which one set of measurements were used to calculate $\langle \ln K_{IC} \rangle$, and a second set were used to determine $\langle n \rangle$ and $\langle \ln \nu_0 \rangle$. If var $(\langle \ln K_{IC} \rangle)$ was determined on p specimens, the number of degrees of freedom for var $(\langle \ln K_{IC} \rangle)$ is $p-1$. If q crack propagation studies were conducted, then the number of degrees of freedom for var $(\langle n \rangle)$ and var $(\langle \ln \nu_0 \rangle)$ is $q-2$. The total number of degrees of freedom, ϕ are then calculated from

$$[\text{var}\,(t\sigma_a^2)]^2/\phi = [(n-2)^2\ \text{var}\,(\langle \ln K_{IC} \rangle)]^2/(p-1) + [\text{var}\,(n, \ln \nu_0)]^2/(q-2) \quad \text{(A12)}$$

where var $(n, \ln \nu_0) = \text{var}\,(\ln t\sigma_a^2) - (n-2)^2$ var $(\langle \ln K_{IC} \rangle)$. A similar treatment is used to determine ϕ from stressing-rate experiments. The expression for ϕ determined by this method will be a function of the variable S/σ_a.

For a given value of S/σ_a, the confidence limits are determined using the expression $\pm t_a$ [var $(\ln t\sigma_a^2)]^{1/2}$. The value of t_a is determined from a Student t-table using the estimate of the number of degrees of freedom calculated from Equation A11. In the present study, 95% confidence limits were calculated for all experimental data.

References

1. S. M. WIEDERHORN, in "Fracture Mechanics of Ceramics" Vol 2, edited by R. C. Bradt, D. P. H. Hasselman, and F. F. Lange (Plenum Press, New York, 1974) pp. 613–45.
2. A. G. EVANS and S. M. WIEDERHORN, *Int. J. Fract.* **10** (1974) 379.
3. S. M. WIEDERHORN, in "Ceramics for High Performance Applications" edited by J. Burke, A. E. Gorum and R. N. Katz (Brook Hill Publishing Co., Chestnut Hill, Mass., 1974) pp. 633–63.
4. J. E. RITTER, Jr, in "Fracture Mechanics of Ceramics" Vol. 4, edited by R. C. Bradt, D. P. H. Hasselman and F. F. Lange (Plenum Press, New York, 1978) pp. 633–86.
5. S. M. WIEDERHORN, E. R. FULLER, Jr, J. MANDEL and A. G. EVANS, *J. Amer. Ceram. Soc.* **59** (1976) 403.
6. S. M. WIEDERHORN and J. E. RITTER, Jr, in Fracture Mechanics Applied to Brittle Materials" ASTM STP 678, edited by S. W. Freiman (American Society for Testing and Materials, Philadelphia, PA, 1979) pp. 202–14.
7. J. E. RITTER, Jr, and J. A. MEISEL, *J. Amer. Ceram. Soc.* **59** (1976) 478.
8. S. M. WIEDERHORN, A. G. EVANS, E. R. FULLER and H. JOHNSON, *ibid* **57** (1974) 319.
9. A. G. EVANS and F. F. LANGE, *J. Mater. Sci.* **10** (1975) 1659.
10. A. G. EVANS and H. JOHNSON *ibid* **10** (1975) 214.
11. R. F. CALDWELL and R. C. BRADT, *J. Amer. Ceram. Soc.* **60** (1977) 168.
12. S. MINDESS and J. S. NADEAU, *Amer. Ceram. Soc. Bull.* **56** (1977) 429.
13. J. E. RITTER, Jr and R. P. LaPORTE, *J. Amer. Ceram. Soc.* **58** (1975) 265.
14. J. E. RITTER, Jr and J. N. HUMENIK, *J. Mater. Sci.* **14** (1979) 626.
15. J. E. RITTER, Jr and K. JAKUS, *J. Amer. Ceram. Soc.* **60** (1977) 171.
16. B. G. KOEPKE, private communication (1979).
17. B. J. PLETKA, E. R. FULLER, Jr and B. G. KOEPKE, in "Fracture Mechanics Applied to Brittle Materials" ASTM STP 678, edited by S. W. Frieman (American Society for Testing and Materials, Philadelphia, PA, 1979) pp. 19–37.
18. A. G. EVANS, *J. Mater. Sci.* 7 (1972) 1137.
19. D. P. WILLIAMS and A. G. EVANS, *J. Test. Eval.* **1** (1973) 264.
20. J. B. WACHTMAN, Jr, W. CAPPS and J. MANDEL, *J. Mater.* 7 (1972) 188.
21. B. J. PLETKA and S. M. WIEDERHORN, in "Fracture Mechanics of Ceramics" Vol 4, edited by R. C. Bradt, D. P. H. Hasselman and F. F. Lange (Plenum Press, New York, 1978) pp. 745–59.
22. G. G. TRANTINA, *J. Amer. Ceram. Soc.* **60** (1977) 338.

23. D. K. SHETTY and A. V. VIRKAR, *ibid* **61** (1978) 93.
24. B. G. KOEPKE, K. D. McHENRY and W. D. SAVAGE, *Amer. Ceram. Soc. Bull.* **58** (1979) 1100.
25. G. K. BANSAL and W. H. DUCKWORTH, *J. Mater. Sci.* **13** (1978) 239.
26. J. E. RITTER, Jr and M. S. CAVANAUGH, *J. Amer. Ceram. Soc.* **57** (1974) 480.
27. M. K. FERBER and S. D. BROWN, *ibid* **63** (1980) 424.
28. A. G. EVANS, M. LINZER and L. R. RUSSELL, *Mater. Sci.Eng.* **15** (1974) 253.
29. T. E. ADAMS, D. J. LANDINI, C. A. SCHUMACHER and R. C. BRADT, *Amer. Ceram. Soc. Bull.* **60** (1981) 730.
30. S. W. FREIMAN, K. R. McKINNEY and H. L. SMITH, in "Fracture Mechanics of Ceramics" Vol. 2, edited by R. C. Bradt, D. P. H. Hasselman and F. F. Lange (Plenum Press, New York, 1974) pp. 659–76.
31. R. F. COOK, B. R. LAWN and G. R. AUSTIS, *J. Mater. Sci.* **17** (1982) 1108.
32. S. W. FREIMAN, private communication (1981).
33. H. HÜBNER and W. JILLEK, *J. Mater Sci.* **12** (1977) 117.
34. P. L. PRATT, in "Fracture 1977" Vol 3, edited by D. M. R. Taplin (University of Waterloo Press, Waterloo, Ontario, Canada 1977) pp. 909–12.
35. G. K. BANSAL and W. H. DUCKWORTH, *J. Mater. Sci.* **13** (1978) 215.
36. M. G. MENDIRATTA and J. J. PETROVIC, *J. Amer. Ceram. Soc.* **61** (1978) 226.
37. D. B. MARSHALL and B. R. LAWN, *ibid* **63** (1980) 532.
38. D. F. JACOBS and J. E. RITTER, Jr, *ibid* **59** (1976) 481.
39. B. L. WALSH, *Biometrika* **34** (1947) 28.

Received 29 June
and accepted 17 August 1981